Study on Recrystallization Softening Behaviour of 23Cr-2.1Ni-10Mn-1.3Mo Economical Duplex Stainless Steels

Chaobo Pu, Yinhui Yang*, Yahui Deng, Ke Ni, Xiaoyu Pan and Zeyao Zeng
School of Materials Science and Engineering, Kunming University of Science and Technology, Kunming, China

Keywords: duplex stainless steel, dynamic recrystallization, deformation softening, critical strain

Abstract: In the temperature range of 1073-1423K and strain rates of 0.01-10s^{-1}, single-pass compression tests were performed on a Gleeble-3800 thermo-mechanical simulator to study the dynamic softening behaviour of 23Cr-2.1Ni-10Mn-1.3Mo low nickel type duplex stainless steel. The flow curves and microstructure showed that the thermal deformation softening was mainly caused by dynamic recovery (DRV) under the condition of high strain rate and low temperature, while Dynamic recrystallization (DRX) softening was mainly occurred at low strain rate. The austenite phase softening changed from DRX to DRV with increasing strain rate at the same temperature. The deformation activation energy *Q* and stress exponent *n* are calculated as 478.83kJ/mol and 5.43, respectively. Combined with Z parameter analysis, DRX was easily to occur under the condition of low Z (1323K, 0.01s^{-1}). The critical strain (stress) and peak strain (stress) obeyed a linear relationship, and the critical strain (stress) decreased with increasing deformation temperature. The linear equations of critical stress (strain) and Z value were obtained by regression analysis.

1 INTRODUCTION

Economical Duplex Stainless Steels (DSS) composing of two phases have an advantageous combination of austenitic and ferritic stainless steel, presenting excellent corrosion resistance and mechanical properties. Therefore, DSS is widely used as a structural material in petrochemicals, marine engineering and energy industries (Charles and Chemelle, 2012; Wan et al., 2014; Mishra et al., 2017). Due to high cost of nickel, the reduction of nickel content in stainless steel under the premise of ensuring material properties is the main way to expand their application. The austenite phase of DSS stabilized by adding low-cost manganese and nitrogen elements to substitute nickel, and maintaining high mechanical properties (Du et al., 2010). It is difficult to add nitrogen in the smelting process of DSS production, but the addition of Mn can effectively stabilize the austenite phase and increase the solid solubility of nitrogen to obtain a two-phase equilibrium structure.

Dynamic recrystallization (DRX) and dynamic recovery (DRV) are significant mechanisms for flow softening during hot processing of metal, which play an important role to control mechanical properties during industrial processing (Frommert and Gottstein, 2009; Meysami and Mousavi, 2011; Chen et al., 2014). In the hot forming processes of DSS, the microstructure evolution is more complicated than a single structure. On account of the difference in two-phase crystal structure and stacking fault energy (SFE) in DSS, the softening mechanism is different during hot deformation. Furthermore, due to different thermal expansion coefficients of ferrite and austenite phases, the stress and strain are unevenly distributed in two phases during the hot forming processes (Siegmund et al., 1995), which easily forms edge and surface cracks (Iza-Mendia et al., 1998). Therefore, optimizing the hot deformation parameters is important for improving hot workability of metals.

As a result, it is important to explore the hot deformation softening behaviour of economical DSS caused by two-phase DRX. The influence of hot deformation parameters on DRX behaviour of high manganese content DSS and the critical characteristic parameters of thermal deformation were studied in this paper. The purpose of this study is to obtain ideal thermal processing parameters, and provide a theoretical reference for development of new nickel type DSS research and actual large production.

Pu, C., Yang, Y., Deng, Y., Ni, K., Pan, X. and Zeng, Z.
Study on Recrystallization Softening Behaviour of 23Cr-2.1Ni-10Mn-1.3Mo Economical Duplex Stainless Steels.
DOI: 10.5220/0008187401840192
In *The Second International Conference on Materials Chemistry and Environmental Protection (MEEP 2018)*, pages 184-192
ISBN: 978-989-758-360-5

2 TESTED PROCEDURE

The chemical compositions of 23Cr-2.1Ni-10Mn-1.3Mo DSS were presented as following (mass%): C 0.0348, Cr 23.388, Mn 10.2748, Ni 2.1279, Si 0.225, S 0.0035, P 0.0063, Mo 1.3527, N 0.2808, Cu 0.1419, Fe(balanced). The tested steel was smelted by vacuum melting furnace, then forged at 1100 ~ 1150℃ into 130 mm wide and 25 mm thick rectangular blocks, finally rolled into 12 mm thick plates. These plates were solution treated at 1050 ℃ for 30 min, and then processed into Φ 8×15 mm compression specimens along the rolling direction. Hot deformation experiments were carried out in Gleeble-3800 thermal-mechanical simulator. The specimens were heated at heating rate of 10 ℃/s to deformation temperature, and held for 3 min to keep microstructure homogenization. The deformation temperatures were performed at 1073, 1173, 1323 and 1423K, respectively, and the deformation strain rates were in the range of 0.01 to 10s^{-1}. In order to keep deformation microstructure, the specimens were taken out quickly and quenched into cold water after each stage of compression. The compressed microstructures were electrolytic etched in concentration HNO_3 with a voltage of 1.5V. The characteristic parameters related to DRX were obtained from the flow curves. The critical strain ε_c, for DRX was calculated from the downward inflection point in the θ ($d\sigma/d\varepsilon$)–σ experimental curves.

3 RESULT AND DISCUSSION

3.1 Flow Behaviour

Figure 1 showed the flow curves under different deformation conditions. It can be found that the flow stress curve transferred from the work hardening stage to the dynamic softening stage under different thermal deformation parameters. The DRX characteristics of flow curves obviously presented with the deformation condition of 0.01-1s^{-1}/1173-1323K, the flow stress falls to the stable value and then becomes flat after reaching the peak value with the increasing of deformation degree (Figure1a-c). The DRX occurred is attributed to higher grain boundary migration rate and DRX nucleation rate.

Deformation at the lower temperature of 1073K, the steady-state flow zone after stress peak decreased and disappeared as the strain rate increased from 0.1 to 10s^{-1}, indicating the deformation softening was mainly caused by DRV. The main reason is that the lower deformation temperature can easily increase the hardening rate of tested DSS. The larger the flow stress, the larger the strain required reaching the peak stress, and the less DRX would occur. In the case of deformation at different strain rates of 1423K, the fluctuation of flow stress with strain after the peak stress is small, which exhibit DRV softening characteristics. The flow curve did not show flow softening feature of DRX at high strain rate of 10s^{-1} (Figure 1d). This is due to the high deformation rate, which leads to insufficient nucleation time and grain growth, thereby inhibiting dynamic recrystallization (Iza-Mendia et al., 1998). Therefore, DRV softening was dominant at high strain rates and low deformation temperatures. But at low strain rates and high temperatures, thermal deformation softening is dominated by DRX.

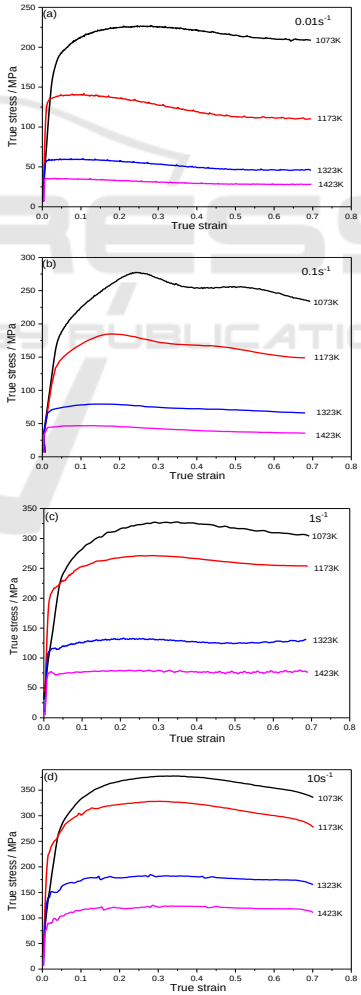

Figure 1: True stress-strain curves of tested steel. (a)0.01s^{-1}; (b)0.1s^{-1} ;(c) 1s^{-1};(d)10s^{-1}.

3.2 Microstructure Evolution

Compared with solution treated microstructure (Figure 2a), it is observed that the compression deformed microstructure has been refined to different degree. The ferrite phase exhibits coarse grained structure at different deformation strain rate and temperature, which mainly caused by DRV due to relatively higher SFE in two phases, while dislocations climbing and cross slipping easily occurred at high deformation temperature. Under the deformation condition of $1s^{-1}$/1173K (Figure 2b), the stripped austenite grain boundary was naturally curved and fine recrystallized sprouting structure appeared, growing gradually with the increasing of deformation temperature (Figure 2c). At higher temperature of 1323K and strain rates of 0.01-$1s^{-1}$, there were a large number of dynamically recrystallized grains that are not sufficiently grown in the austenite (Figure 2d, e), and the grain size of recrystallization increases with increasing strain rate. For sample deformed at strain rate of $10s^{-1}$(Figure 2f), the grain boundaries of austenite phases gradually became flat and stable, and enlarged grain size distribution difference due to the occurrence between DRV and partial DRX. Therefore, the austenitic phase deformation changed from DRX to DRV with increasing strain rate at the same temperature, which is consistent with the analysis of true stress-strain curves.

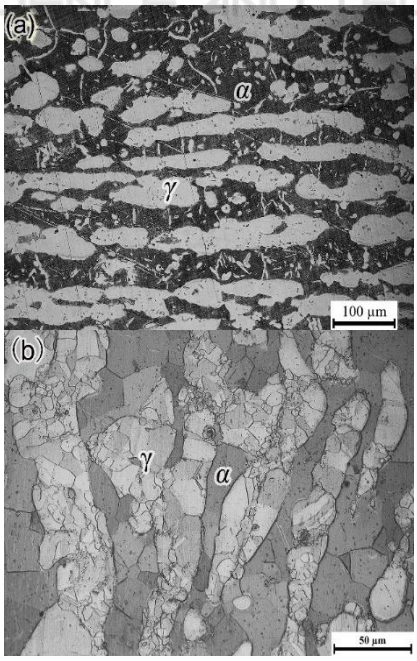

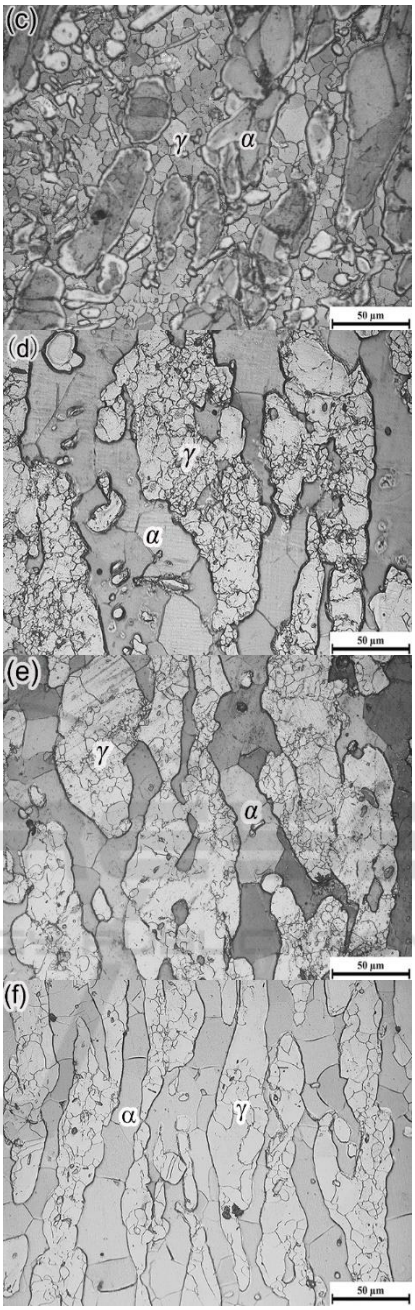

Figure 2: Typical OM images of tested steel under different deformation conditions. (a) Solution treated sample; (b) T=1173K, $\dot{\varepsilon}$ =$1s^{-1}$; (c) T=1323K, $\dot{\varepsilon}$ =$1s^{-1}$; (d) T=1323K, $\dot{\varepsilon}$ =$0.01s^{-1}$; (e) T=1323K, $\dot{\varepsilon}$ =$0.1s^{-1}$; (f) T=1323K, $\dot{\varepsilon}$ =$10s^{-1}$.

3.3 Constitutive Equations for Flow Behaviour

The activation energy Q is an important parameter reflecting hot deformation difficulty for metal

material, which determines the critical condition of DRX. The relation between the flow stress, deformation temperature and strain rate of hot deformation can be analyzed and described by the mathematical model, named the Arrhenius equation characterized by the zener-hollomon parameter (Z) (Xu et al., 2013).

$$\dot{\varepsilon} = AF(\sigma)exp(-\frac{Q}{RT}) \quad (1)$$

$$Z = \dot{\varepsilon}exp\left(\frac{Q}{RT}\right) \quad (2)$$

Where Z is the temperature compensated strain rate, $\dot{\varepsilon}$ is the strain rate, A is the tested constant, Q is the apparent deformation activation energy, R is the gas constant, T is the thermodynamic temperature. While $F(\sigma)$ is a function of flow stress with the following equations (Haghdadi et al., 2016; Wang et al., 2013):

$$F(\sigma) = \sigma^{n_1} \qquad \alpha\sigma < 0.8 \quad (3)$$

$$F(\sigma) = exp(\beta\sigma) \qquad \alpha\sigma > 1.2 \quad (4)$$

$$F(\sigma) = [sinh(\alpha\sigma)]^n \qquad \forall\sigma \quad (5)$$

α, β, n and n_1 are material constants and $\alpha = \beta / n_1$.

Considering that in a certain temperature, when Q is independent of T, thus the Eqs. (6) and (7) can be obtained by substituting Eq. (3) and (4) to Eq. (1) respectively:

$$\dot{\varepsilon} = B\sigma^{n_1}exp(-\frac{Q}{RT}) \quad (6)$$

$$\dot{\varepsilon} = Cexp(\beta\sigma)exp(-\frac{Q}{RT}) \quad (7)$$

Where B and C are material constants, independent of temperature. Taking the natural logarithm of both sides of Eqs. (6) and (7), it can be obtained as following equations:

$$\ln\sigma = \frac{1}{n_1}\ln(\dot{\varepsilon}) - \frac{1}{n_1}\ln B + \frac{1}{n_1}\frac{Q}{RT} \quad (8)$$

$$\sigma = \frac{1}{\beta}\ln(\dot{\varepsilon}) - \frac{1}{\beta}\ln C + \frac{1}{\beta}\frac{Q}{RT} \quad (9)$$

It is easy to obtain the value of n_1, β from the slop of the plots shown in Figure3 (a) and (b) ($\ln\sigma$ versus $\ln\dot{\varepsilon}$ and σ versus $\ln\dot{\varepsilon}$) based on Eqs. (8) and (9). The value of constant parameters are showed as: n_1 = 8.2432, β = 0.0536, $\alpha = \beta / n_1$ = 0.0065. Substituting Eq. (5) into the Eq. (1) yields Eq. (10), then taking the natural logarithm, the Eqs. (11) and (12) were obtained.

$$\dot{\varepsilon} = A[sinh(\alpha\sigma)]^n exp(-\frac{Q}{RT}) \quad (10)$$

$$\ln[sinh(\alpha\sigma)] = \frac{1}{n}\ln(\dot{\varepsilon}) - \frac{1}{n}\ln A + \frac{Q}{nRT} \quad (11)$$

$$\ln[sinh(\alpha\sigma)] = \frac{1}{T}\frac{Q}{nR} + \frac{1}{n}(\ln(\dot{\varepsilon}) - \ln A) \quad (12)$$

The hot deformation constant n and active energy Q can be derived from the Arrhenius plots of Figure3 (c) and (d) ($\ln[\sinh(\alpha\sigma)]$ versus $\ln(\dot{\varepsilon})$ and $\ln[\sinh(\alpha\sigma)]$ versus $(1/T)$). Thus, the Q and n values of tested steel are calculated as 418.83 kJ / mol and 5.4357, respectively.

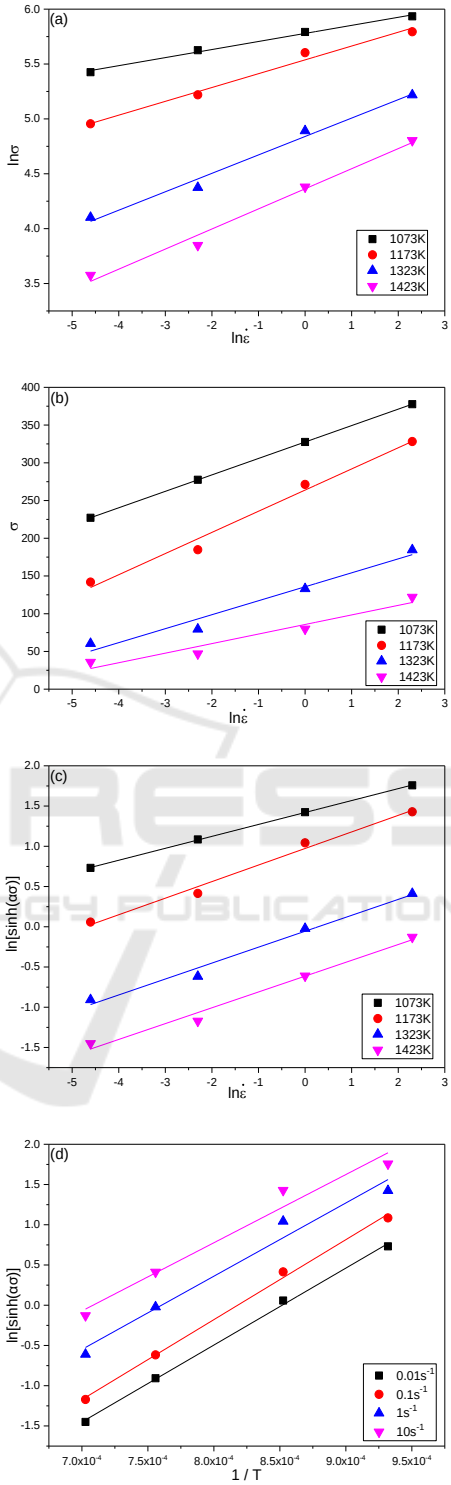

Figure 3: Relationship between peak stress and deformation rate with temperature. (a) $\ln\sigma$ versus $\ln\dot{\varepsilon}$; (b) σ versus $\ln\dot{\varepsilon}$; (c) $\ln[\sinh(\alpha\sigma)]$ versus $\ln\dot{\varepsilon}$; (d) $\ln[\sinh(\alpha\sigma)]$ versus $1/T$.

The expression of the Z parameter of the deformation process of the tested steel can be obtained by the acquired activation energy *Q*, combined with the Eqs. (1), (2) and (5):

$$Z = \dot{\varepsilon} exp\left(\frac{Q}{RT}\right) = A[sinh(\alpha\sigma)]^n \quad (13)$$

Taking the natural logarithms on both sides of Eq. (13), then Eq. (14) can be obtained.

$$\ln Z = \ln A + n\ln[sinh(\alpha\sigma)] \quad (14)$$

According to the relationship curves of $\ln[\sinh(\alpha\sigma)]$ and $\ln\dot{\varepsilon}$ (Figure 4), the average value of *A* can be estimated to be 3.1856×10^{16} for the tested steel. The Eq. (14) can be expressed as follow by the nature of the hyperbolic sine function:

$$\left(\frac{Z}{A}\right)^{\frac{1}{n}} = \sinh(\alpha\sigma) = \frac{e^{\alpha\sigma}-e^{-\alpha\sigma}}{2} \quad (15)$$

The peak stress constitutive equation can be solved as the follow expression:

$$\sigma = \frac{1}{\alpha}\ln\left\{\left(\frac{Z}{A}\right)^{\frac{1}{n}} + \left[\left(\frac{Z}{A}\right)^{\frac{2}{n}} + 1\right]^{\frac{1}{2}}\right\} \quad (16)$$

As a result, the hot deformation equation of tested steel is shown as Eq. (17), and the flow stress constitutive equation are expressed as Eq. (18).

$$\dot{\varepsilon} = 3.1856 \times 10^{16}[sinh(0.0065\sigma)]^{8.2432} \times exp\left(\frac{-418830}{8.314\times T}\right) \quad (17)$$

$$\sigma = \frac{1}{0.0065}\ln\left\{\left(\frac{Z}{3.1856\times10^{16}}\right)^{\frac{1}{5.4357}} + \left[\left(\frac{Z}{3.1856\times10^{16}}\right)^{\frac{2}{5.4357}} + 1\right]^{\frac{1}{2}}\right\} \quad (18)$$

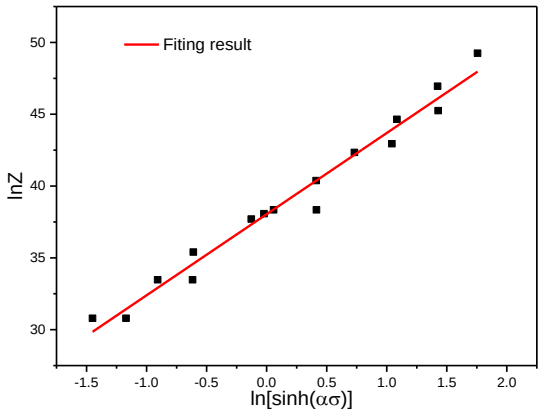

Figure 4: Relationship between lnZ and ln[sinh(ασ)].

Z parameters were introduced comprehensively to describe the flow behaviour of tested steel at a certain deformation temperature and strain rate. The smaller the Z value is, the smaller deformation resistance and the higher mobility of dislocations and grain boundaries are, as well as the greater tendency for DRX is during deformation. Some fine grains sprouted from the austenite phase (Figure 2d) at a small Z value (such as 1323K, $0.01s^{-1}$), indicating the occurrence of DRX. On the contrary, the larger Z value is, the higher deformation resistance is, the smaller driving force is for recrystallization, so the smaller tendency to recrystallize is. It can be seen from Figure 2b that under the condition of the maximum Z value (such as 1173K, $1s^{-1}$), DRV is main softening behaviour.

3.4 Critical Condition Model for DRX

The critical strain (ε_c) of material is the prerequisite for the research on DRX, which usually was activated before the peak stress (Imbert and Mcqueen, 2001). The inflections in the plot of strain hardening rate ($\theta=\partial\sigma/\partial\varepsilon$) versus flow stress ($\sigma$) are attributed to DRX, which not only characterizes the microstructure evolution during the deformation processing, but also determines the characteristic values of the deformation resistance accurately (Chen et al., 2016).

The strain hardening rate decreases sharply with increasing of temperature at a low strain rate of $0.1s^{-1}$ (Figure 5a), which is because that the low dislocation energy at low temperature region increases work hardening. In the high temperature region, with the increasing of dislocation energy, the stress relaxation due to more dislocations migration greatly reduced strain hardening rate. At high strain rate of $10s^{-1}$ (Figure 5c), the strain hardening rate in the high temperature zone was higher than that deformed at $0.1s^{-1}$, indicating that the work hardening was dominant in the flow process under the high strain rate. The strain hardening rate increased with the increasing of deformation rate at a lower deformation temperature of 1073K (Figure 5d). However, the strain hardening rate increases first and then decreases with the increasing of strain rate at a higher temperature of 1323K (Figure 5f).

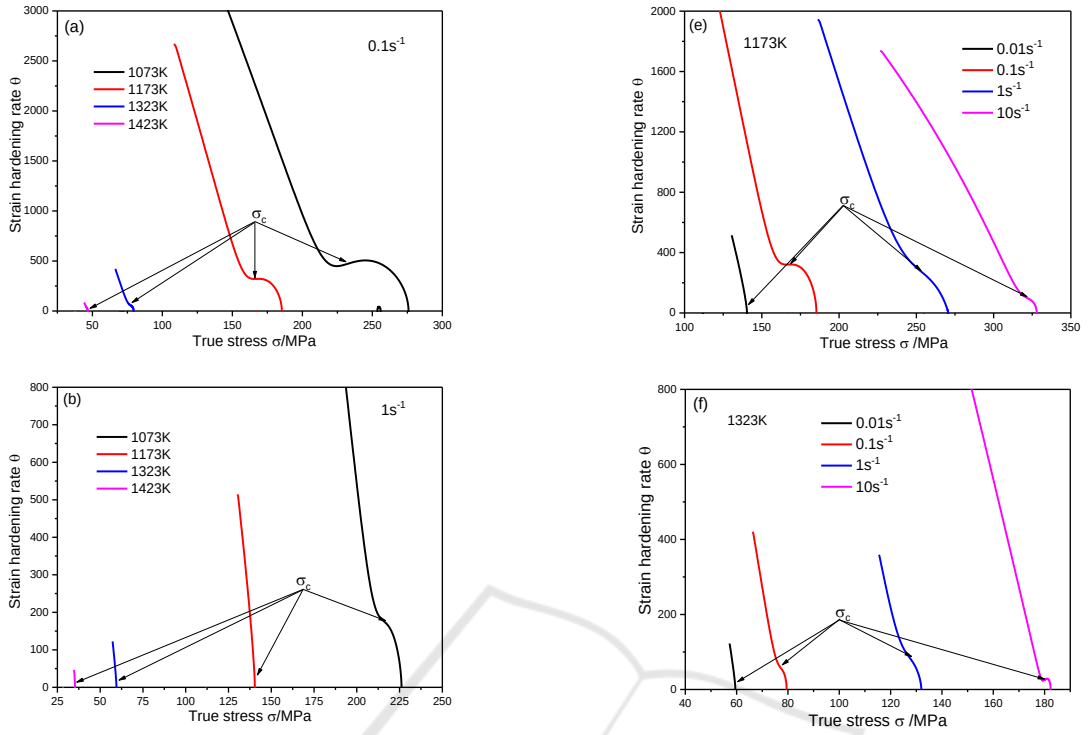

Figure 5: Strain hardening rate versus flow stress under different deformation conditions. (a) $0.1s^{-1}$; (b) $1s^{-1}$; (c) $10s^{-1}$; (d) 1073K; (e) 1173K; (f) 1323K.

Table 1: The data of characteristic points in flow curves under different conditions.

Strain rate	Temperature/K	ε_c	ε_p	σ_c/MPa	σ_p/MPa
$0.01s^{-1}$	1073	0.110	0.235	215.14	226.13
	1173	-	0.109	-	140.38
	1323	-	0.087	-	59.612
	1423	-	0.063	-	35.622
$0.1s^{-1}$	1073	0.128	0.228	238.65	276.17
	1173	0.098	0.178	168.55	184.79
	1323	0.076	0.143	76.463	79.396
	1423	0.066	0.121	46.36	46.826
$1s^{-1}$	1073	0.128	0.288	296.13	327.02
	1173	0.115	0.240	255.48	270.59
	1323	0.105	0.184	125.87	132.42
	1423	0.101	0.176	76.416	78.911
$10s^{-1}$	1073	0.146	0.322	354.202	377.572
	1173	0.122	0.273	312.05	327.79
	1323	0.113	0.247	117.42	181.72
	1423	0.091	0.175	114.56	119.38

The characteristic points of the flow curves under different deformation conditions are shown in Table 1. It can be seen that under the condition of 0.1 -10s^{-1}, the peak stress and the critical stress decreased with increasing temperature at the same strain rate, which is caused by the increasing of the energy provided by the increasing of temperature. The critical strain also decreased with increasing of deformation temperature. In the low temperature region of 1073 - 1173K, the critical strain increased with the increasing of deformation rate. This is because the deformation energy storage of the material increases with increasing strain rate, and the energy consumption increases. The critical strain increased first and then decreased with the increasing of strain rate at 1423K, indicating that the strain rate of 1s^{-1} is the turning point of the hot processing.

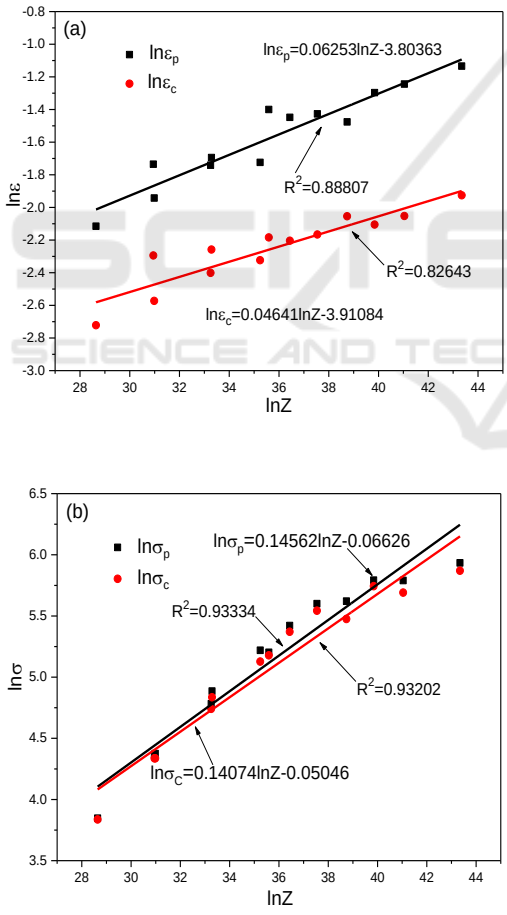

Figure 6: Relationship between (a) $\ln\varepsilon_p$, $\ln\varepsilon_c$ and Z; (b) $\ln\sigma_p$, $\ln\sigma_c$ and lnZ.

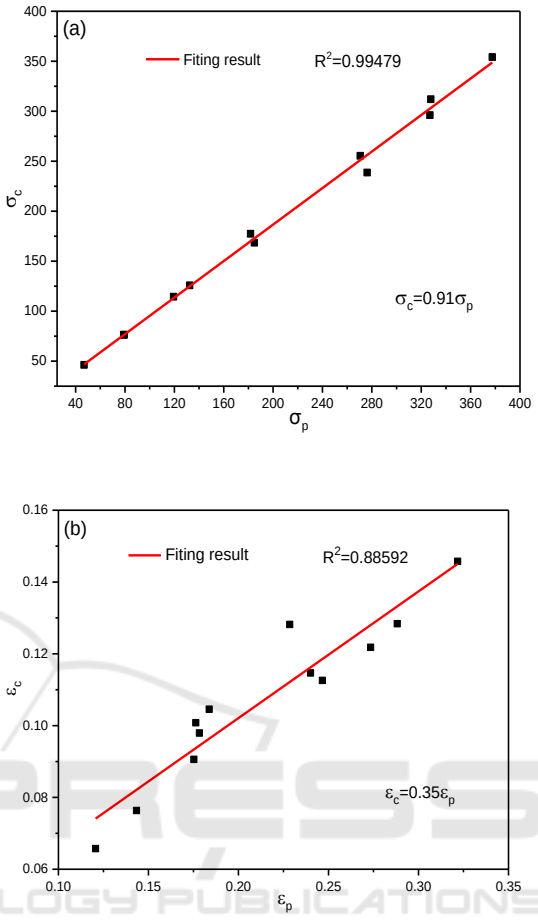

Figure 7: Relationship between (a) σ_p and σ_c; (b) ε_p and ε_c.

As shown in Figure 6, it can be seen that the critical strain (stress) and peak strain (stress) increase with the increasing of Z value, showing a better linear relationship. Regression analysis of these curves resulted in the following equation:

$$\ln\varepsilon_p=0.06253\ln Z-3.80363 \quad (19)$$

$$\ln\varepsilon_c=0.04641\ln Z-3.91084 \quad (20)$$

$$\ln\sigma_p=0.14562\ln Z-0.06626 \quad (21)$$

$$\ln\sigma_c=0.14074\ln Z-0.05046 \quad (22)$$

The relationship between ε_c (σ_c) and ε_p (σ_p) is plotted in Figure 7. It can be observed that the dependence of ε_c (σ_c) on ε_p (σ_p) obeys a linear equation and the following equations are obtained.

$$\sigma_c = 0.91\ \sigma_p \quad (23)$$

$$\varepsilon_c = 0.35\ \varepsilon_p \quad (24)$$

The ratio of ε_c to ε_p has been reported to be 0.43 for austenitic stainless steel, the general range reported for steels is between 0.3 and 0.9, (Chen et al., 2016) the ratio of σ_c to σ_p often takes values between 0.83 (Wang et al., 2013) and 0.90 (Zhao et al., 2014). So the values 0.35 and 0.91 are in reasonable.

4 CONCLUSIONS

In this paper, the compression recrystallization softening behaviour of 23Cr-2.1Ni-10Mn-1.3Mo economical duplex stainless steel was investigated. The main results can be summarized as follow:

(1) The austenite phase changes from dynamic recrystallization to dynamic recovery with the increasing of strain rate at the same deformation temperature.

(2) The relationship between peak stress (strain) and critical stress (strain) is: σ_c=0.91 σ_p and ε_c=0.35 ε_p. The critical strain in the low temperature zone increases with the increasing of deformation temperature and strain rate, which increases first and then decreases in the high temperature zone. Combing with the Z parameter, DRX was prone to occur under low Z conditions and DRV occurred easily under high Z conditions.

(3) The thermal deformation and constitutive equation of tested steel are shown as follow respectively :

$$\dot{\varepsilon} = 3.1856 \times 10^{16}[sinh(0.0065\sigma)]^{8.2432} \times exp\left(\frac{-418830}{8.314 \times T}\right)$$

$$\sigma = \frac{1}{0.0065}\ln\left\{\left(\frac{Z}{3.1856 \times 10^{16}}\right)^{\frac{1}{5.4357}} + \left[\left(\frac{Z}{3.1856 \times 10^{16}}\right)^{\frac{2}{5.4357}} + 1\right]^{\frac{1}{2}}\right\}$$

(4) The relationship between characteristic points and flow stress on Z was obtained as $\ln\varepsilon_p$ = 0.06253 lnZ-3.80363, $\ln\varepsilon_c$ = 0.04641 lnZ-3.91084, $\ln\sigma_p$ = 0.14562 lnZ-0.06626 and $\ln\sigma_c$ = 0.14074 lnZ-0.05046.

ACKNOWLEDGEMENTS

This study was financially supported by the National Natural Science Foundation of China (NSFC Project no. 51461024).

REFERENCES

Charles, J., Chemelle, P., 2012. The history of duplex developments, nowadays DSS properties and duplex market future trends [J]. *World. Iron. Steel.*, 144(2): 477.

Chen, L., Zhang, Y., Li, F. et al., 2016. Modeling of dynamic recrystallization behavior of 21Cr-11Ni-N-RE lean austenitic heat-resistant steel during hot deformation [J]. *Mater. Sci. Eng., A*, 663: 141-150.

Chen, X. M., Lin, Y. C., Wen, D. X. et al., 2014. Dynamic recrystallization behavior of a typical nickel-based superalloy during hot deformation [J]. *Mater. Des.*, 2014, 57(5): 568-577.

Du, C. F., Zhan, F., Yang, Y. H. et al., 2010. Research progress and application of double phase stainless steel [J]. *Met. Funct. Mater*., 17(05): 63.

Frommert, M., Gottstein, G., 2009. Mechanical behavior and microstructure evolution during steady-state dynamic recrystallization in the austenitic steel 800H [J]. *Mater. Sci. Eng. A*., 506(1): 101-110

Haghdadi, N., Martin, D., Hodgson, P., 2016. Physically-based constitutive modelling of hot deformation behavior in a LDX 2101 duplex stainless steel ☆ [J]. *Mater. Des*., 106: 420 - 427.

Imbert, C. A. C., Mcqueen, H. J., 2001. Peak strength, strain hardening and dynamic restoration of A2 and M2 tool steels in hot deformation [J]. *Mater. Sci. Eng. A*., 313(1): 88-103.

Iza-Mendia, A., Piñol-Juez, A., Urcola, J. J. et al., 1998. Microstructural and mechanical behavior of a duplex stainless steel under hot working conditions [J]. *Metall. Mater. Trans. A*., 29(12): 2975-2986.

Meysami, M., Mousavi, S. A. A. A., 2011. Study on the behavior of medium carbon vanadium microalloyed steel by hot compression test [J]. *Mater. Sci. Eng. A*., 528(7): 3049-3055.

Mishra, M. K., Balasundar, I., Rao, A. G. et al., 2017. On the High Temperature Deformation Behaviour of 2507 Super Duplex Stainless Steel [J]. *J. Mater. Eng. Perform.*, 26(2): 1- 11.

Siegmund, T., Werner, E., Fischer, F. D., 1995. On the thermomechanical deformation behavior of duplex-type materials [J]. *J. Mech. Phys. Solids*., 43(4): 495-532.

Wan, J., Ran, Q., Li, J. et al., 2014. A new resource-saving, low chromium and low nickel duplex stainless steel 15Cr– x Al–2Ni– y Mn [J]. *Mater. Des.*, 53(1): 43-50.

Wang, M. H., Li, Y. F., Wang, W. H. et al., 2013. Quantitative analysis of work hardening and dynamic

softening behavior of low carbon alloy steel based on the flow stress [J]. *Mater. Des.*, 45: 384-392.

Xu, D., Zhu, M., Tang, Z. et al., 2013. Determination of the dynamic recrystallization kinetics model for SCM435 steel [J]. *Journal of Wuhan University of Technology (Materials Science Edition)*, 28(4): 819-824

Zhao, B., Zhao, T., Li, G., et al., 2014. The kinetics of dynamic recrystallization of a low carbon vanadium-nitride microalloyed steel [J]. *Mater. Sci. Eng., A*, 604: 117-121.